Statistical Analysis for Shielding Effectiveness Measurement of Materials Using Reverberation Chambers

Wenjun Qi, Kai Chen, Xueqi Shen, Yongjiu Zhao, Qian Xu, *Member, IEEE*, Tian Hong Loh, *Senior Member, IEEE*, and Yi Huang, *Fellow, IEEE*

***Abstract*—Statistical analysis for material shielding effectiveness (SE) measurement in a nested reverberation chamber (RC) and a contiguous RC is given in this article. By using Mellin transform and the associated statistical methods, the corresponding analytical expressions of the SE are derived, respectively, for the sample material under test with good and poor electromagnetic shielding performance. Moreover, the probability density function, the expected value, and the standard deviation of SE in different scenarios using nested and contiguous RCs are obtained analytically. Monte Carlo simulation and measurements in nested and contiguous RCs are performed to verify the analytical expressions.**

***Index Terms*—Contiguous reverberation chamber (RC), nested RC, shielding effectiveness (SE), statistical analysis.**

I. Introduction

SHIELDING effectiveness (SE) is an important figure of merit to assess the electromagnetic shielding properties of materials [1], [2]. During these years, various methods have been introduced and standardized for SE testing [3], [4], [5], [6], [7], [8], [9], [10], [11], [12], [13], [14]. A reverberation chamber (RC) is an electrically large shielded cavity, which has been widely applied to electromagnetic compatibility testing [15], [16], [17] and over-the-air testing [18], [19], [20]. The SE measurements of material under test (MUT) in an RC are superior over other methods because an RC offers a more realistic and complex environment as compared with an anechoic chamber that envisaged to offer an ideal reflectionless environment. Measurement samples in an RC are illuminated with electromagnetic fields with random polarizations and angles of incidence.

Generally, the typical measurement procedure for the SE measurement is to compare the measured transfer functions with and without the shielding materials, which is performed in nested or contiguous RCs [21], [22], [23]. In [3], a better way to define the SE for the MUT using nested RCs was proposed. Compared with the conventional definitions [24], [25], in this method, the effective transmission cross section is obtained, and the value of SE is basically a function of material properties.

Since the RC can generate a statistically uniform, isotropic, and randomly polarized electromagnetic field, statistical analysis and uncertainty calculation should be performed on the measured physical quantities. Researchers have greatly used statistical analyses in RCs, such as electromagnetic fields in nested RCs [26], Q factor [27], [28], antenna efficiency [29], [30], [31], and enhanced backscatter coefficient [32]. The relevant analytical expressions for many statistics quantities (such as mean, variance, and unbiased estimators) can be obtained. However, limited work has been performed to investigate the statistical analysis of the material SE.

This work focuses on the statistical analysis of the material SE measurement in different scenarios using nested and contiguous RCs. The probability density functions (PDFs) and cumulative distribution functions (CDFs) of SE can be derived. It is interesting to find that the PDF and CDF depend on the value of measured SE as the electromagnetic distributions are different for MUT with good and poor electromagnetic shielding performance. The derived statistics are verified using numerical simulations as well as RC measurements.

The rest of this article is organized as follows. Section II reviews the testing procedure of SE and derives the analytical expressions for different cases in an RC; the Monte Carlo simulation are also conducted for the different MUT. The measurements in the nested and contiguous RC are performed to

Manuscript received 22 May 2022; revised 29 August 2022 and 17 October 2022; accepted 13 November 2022. This work was supported in part by Nanjing Rongce Testing Technology Ltd., in part by the 2021–2025 National Measurement System Programme of the U.K. Government's Department for Business, Energy and Industrial Strategy, Science Theme Reference EMT22, in part by the National Defense Basic Scientific Research Program of China under Grant JCKYS2021DC05, and in part by the Fund of Prospective Layout of Scientific Research for NUAA. *(Corresponding author: Qian Xu.)*

Wenjun Qi, Yongjiu Zhao, and Qian Xu are with the College of Electronic and Information Engineering, Nanjing University of Aeronautics and Astronautics, Nanjing 211106, China (e-mail: qiwenjun@nuaa.edu.cn; yjzhao@nuaa.edu.cn; emxu@foxmail.com).

Kai Chen is with the College of Electronic and Information Engineering, Nanjing University of Aeronautics and Astronautics, Nanjing 211106, China, and also with the Nanjing Rongce Testing Technology Ltd., Nanjing 211112, China (e-mail: chenkay@nuaa.edu.cn).

Xueqi Shen is with the Nanjing Rongce Testing Technology Ltd., Nanjing 211112, China (e-mail: george@emcdir.com).

Tian Hong Loh is with the Electromagnetic & Electrochemical Technologies Department, Electromagnetic Technologies Group, National Physical Laboratory, Teddington TW11 0LW, U.K. (e-mail: tian.loh@npl.co.uk).

Yi Huang is with the Department of Electrical Engineering and Electronics, University of Liverpool, Liverpool L69 3GJ, U.K. (e-mail: yi.huang@liv.ac.uk).

Color versions of one or more figures in this article are available at https://doi.org/10.1109/TEMC.2022.3223996.

Digital Object Identifier 10.1109/TEMC.2022.3223996

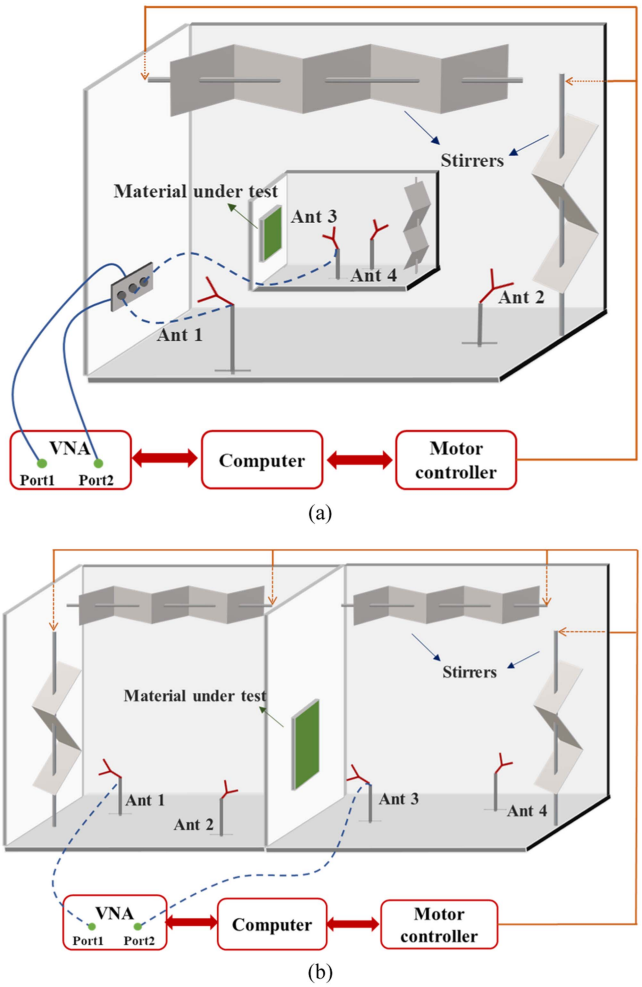

Fig. 1. Configuration for SE measurement (a) in a nested RC and (b) in a contiguous RC.

verify the analytical distributions of SE in Section III. Finally, Section IV concludes this study.

II. Statistics Analysis of SE

Typical configuration setups of the SE measurement in a nested RC and a contiguous RC are shown in Fig. 1(a) and (b), respectively. A vector network analyzer (VNA) is used to measure the scattering parameters (*S*-parameters). A computer is used to control the VNA and the rotation of stirrers. One supposes that Ant 1 is used as the transmitting (Tx) antenna, and Ant 2, which is used as the receiving (Rx) antenna, is far from Ant 1 in the outer/left chamber. Ant 3 and Ant 4 are the Rx antenna and Tx antenna in the inner/right chamber. The SE of a MUT can be expressed using measured *S*-parameters [3]:

$$\mathrm{SE} = -10\log_{10}\frac{\left\langle |S_{21\mathrm{ns}}|^2\right\rangle_N \left\langle |S_{31\mathrm{ws}}|^2\right\rangle_N \left\langle |S_{34\mathrm{ns}}|^2\right\rangle_N}{\left\langle |S_{21\mathrm{ws}}|^2\right\rangle_N \left\langle |S_{31\mathrm{ns}}|^2\right\rangle_N \left\langle |S_{34\mathrm{ws}}|^2\right\rangle_N} \quad (1)$$

where the subscript "ws" represents "with sample," and "ns" represents "no sample" of the measured *S*-parameters. $\langle\cdot\rangle_N$ represents the average operation, which is taken over different stirring sequences. Equation (1) requires a reciprocal MUT and chambers sufficiently isolated [23], [33]. It is interesting to note that, for the MUT with good and poor electromagnetic shielding performance, the distribution of $|S_{31\mathrm{ws}}|$ in (1) is different. For the MUT with good electromagnetic shielding performance, the electromagnetic distributions of the two chambers are independent of each other. However, when the SE of MUT is not good, the electric field (E-field) in a nested RC is Rayleigh distribution. As shown in Fig. 2, the PDFs of the Rayleigh distribution and the double Rayleigh distribution are given. The double Rayleigh distribution can be seen as a product of two Rayleigh distributions. The difference of these two distributions influences the expression of the SE. For nonperfect uniformity of the fields inside the RCs, Rician distribution could be used to model the PDFs with different K-factors. Note that the measurement uncertainty could be reduced by performing measurements in more than one position/polarization of the antenna(s). However, analytical expressions could not be available. For the frequencies lower than the LUF, different RCs may have different PDFs, which make it more difficult to describe. In this article, we limit our research to the region of overmoded and well-stirred conditions.

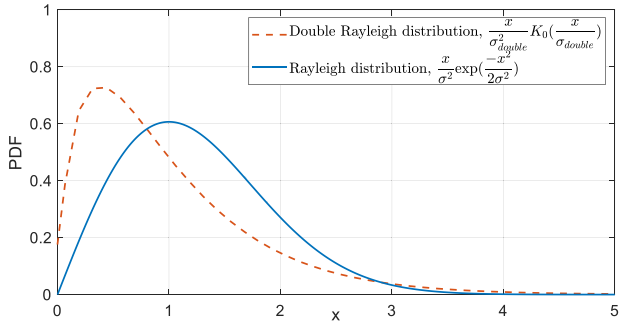

Fig. 2. PDF of the Rayleigh distribution and double Rayleigh distribution; the mean values are normalized to 1.

In this section, we start from (1) and end with (12)–(15), (20), and (21). Note that the linear units are used, not the log form.

A. MUT With Poor Electromagnetic Shielding Performance

For the MUT with poor electromagnetic shielding performance, the E-field in the inner chamber, as well as in the outer chamber, is spatially Rayleigh distributed. It is well known that the term $|S_{21\mathrm{ns}}|^2$ is envisaged to have an exponential distribution [17], and the relevant PDF can be expressed as

$$p_X\ (x) = \frac{1}{T_{21\mathrm{ns}}}e^{-x/T_{21\mathrm{ns}}},\ X = |S_{21\mathrm{ns}}|^2 \quad (2)$$

where $T_{21\mathrm{ns}}$ represents both the mean value and the standard deviation value. Similarly, the $|S_{31\mathrm{ws}}|^2$, $|S_{34\mathrm{ns}}|^2$, $|S_{21\mathrm{ws}}|^2$, $|S_{31\mathrm{ns}}|^2$, and $|S_{34\mathrm{ws}}|^2$ have the same PDF expression. The mean value and the standard deviation value are also expressed as $T_{31\mathrm{ws}}$, $T_{34\mathrm{ns}}$, $T_{21\mathrm{ws}}$, $T_{31\mathrm{ns}}$, and $T_{34\mathrm{ws}}$. The PDF of $\langle|S_{21\mathrm{ns}}|^2\rangle$ from N

independent samples can be derived as

$$p_{X_n}\ (x_n) = \frac{\left(\frac{N}{T_{21\text{ns}}}\right)^N}{\Gamma\left(N\right)}\ x_n^{N-1} e^{-\frac{x_n N}{T_{21\text{ns}}}},\quad X_n = \left\langle \left|S_{21\text{ns}}\right|^2 \right\rangle_N. \tag{3}$$

Equation (3) is the PDF of the random variable x_n, which is Gamma distribution or Erlang distribution. The mean value is still $T_{21\text{ns}}$, and the standard deviation is $T_{21\text{ns}}/\sqrt{N}$. Moreover, one replaces $T_{21\text{ns}}$ with $T_{21\text{ws}}$, the PDF of $1/x_n$, $p_{X_{n'}}(x_{n'})$, is denoted as

$$p_{X_{n'}}\ (x_{n'}) = \frac{\left(N/T_{21\text{ws}}\right)^N}{\Gamma\left(N\right) x_{n'}^{N+1}}\ e^{-\frac{N}{x_{n'} T_{21\text{ws}}}},\quad X_{n'} = \frac{1}{\left\langle \left|S_{21\text{ws}}\right|^2 \right\rangle_N} \tag{4}$$

the mean value is $N/[T_{21\text{ws}}(N-1)]$, and the standard deviation is $N/[T_{21\text{ws}}\ (N-1)\sqrt{N-2}\,]$. Here, the Mellin transform (integral transform) is utilized to derive the analytical expression of (1). The Mellin transform of function $f(t)$ is defined as [34], [35]

$$M\ (s) = \mathcal{M}\ [f\ (t)] = \int_0^\infty f\ (t)\, t^{s-1} dt \tag{5}$$

where *s* is in the complex domain. The inverse Mellin transform is given as

$$f\ (t) = \mathcal{M}^{-1}\ \ [M\ (s)] = \frac{1}{2\pi j}\ \int_{C-j\infty}^{C+j\infty} M\ (s)\, t^{-s} ds \tag{6}$$

and C is a real number. Noting that the Mellin transform of the PDF of a product of random variables $X \times Y$ is the product of the Mellin transforms of the PDF of individual random variables, and the expression is

$$M_{XY}\ (s) = M_X\ (s)\, M_Y\ (s) \tag{7}$$

the mean value is $M_{XY}(2)$ and the variance value is $M_{XY}(3) - M_{XY}^2(2)$.

$$\begin{aligned} \mathcal{M}\left[p_{X_n}\left(x_n\right)\right] &= \int_0^\infty p_{X_n}\left(x_n\right) x_n^{s-1} dx_n \\ &= \frac{\Gamma\left(N+s-1\right)}{\Gamma\left(N\right)}\ \left(\frac{T_{21\text{ns}}}{N}\right)^{s-1} \end{aligned} \tag{8}$$

and

$$\begin{aligned} \mathcal{M}\left[p_{X_{n'}}\left(x_{n'}\right)\right] &= \int_0^\infty p_{X_{n'}}\left(x_{n'}\right) x_{n'}^{s-1} dx_{n'} \\ &= \frac{\Gamma\left(N-s+1\right)}{\Gamma\left(N\right)}\ \left(\frac{N}{T_{21\text{ws}}}\right)^{s-1} \end{aligned} \tag{9}$$

where $\Gamma(\cdot)$ is the Gamma function. The PDF of the product $\left|S_{21\text{ns}}\right|^2$, $\left|S_{31\text{ns}}\right|^2$, $\left|S_{34\text{ns}}\right|^2$, $1/\left|S_{21\text{ws}}\right|^2$, $1/\left|S_{31\text{ws}}\right|^2$, and $1/\left|S_{34\text{ws}}\right|^2$ of using the Mellin transform is derived as

$$\begin{aligned} \mathcal{M}\left[p_{X_{\text{SE}}}\left(x_{\text{SE}}\right)\right] &= \int_0^\infty p_{X_{\text{SE}}}\left(x_{\text{SE}}\right) x_{\text{SE}}^{s-1} dx \\ &= \frac{\Gamma(N+s-1)^3 \Gamma(N-s+1)^3}{\Gamma(N)^6} \end{aligned}$$

$$\left(\frac{T_{21\text{ns}} T_{31\text{ws}}\ T_{34\text{ns}}}{T_{21\text{ws}} T_{31\text{ns}}\ T_{34\text{ws}}}\right)^{s-1} \tag{10}$$

where X_{SE} is defined as

$$\frac{\left\langle \left|S_{21\text{ns}}\right|^2 \right\rangle_N \left\langle \left|S_{31\text{ws}}\right|^2 \right\rangle_N \left\langle \left|S_{34\text{ns}}\right|^2 \right\rangle_N}{\left\langle \left|S_{21\text{ws}}\right|^2 \right\rangle_N \left\langle \left|S_{31\text{ns}}\right|^2 \right\rangle_N \left\langle \left|S_{34\text{ws}}\right|^2 \right\rangle_N}. \tag{11}$$

Using the inverse Mellin transform, the PDF of the random variable is obtained as

$$\begin{aligned} &p_{X_{\text{SE}}}\left(x_{\text{SE}}\right) \\ &= \frac{\text{MeijerG}\left[\{\{-N,-N,-N\},\{\,\}\},\{\{-1+N,-1+N,-1+N\},\{\,\}\},\frac{x_{\text{SE}}}{R}\right]}{R\Gamma(N)^6} \end{aligned}$$

where

$$R\ = \frac{T_{21\text{ns}} T_{31\text{ws}}\ T_{34\text{ns}}}{T_{21\text{ws}} T_{31\text{ns}}\ T_{34\text{ws}}} \tag{12}$$

and

$$\begin{aligned} &\text{MeijerG}\Big[\ \{\{-N,-N,-N\}\,,\{\,\}\}\,,\{\{-1+N,-1+N,\\ &-1+N\}\,,\{\,\}\}\,,\frac{x_{\text{SE}}}{R}\Big] \\ &= \frac{1}{2\pi j}\ \int_L^\Gamma (1+N-s)^3 \Gamma(-1+N+s)^3 \Big(\frac{x_{\text{SE}}}{R}\Big)^{-s} ds \end{aligned} \tag{13}$$

where L is the integral path in [29]. Therefore, when $s = 2$, the mean value of (10) is obtained as

$$\mu\ \left(x_{\text{SE}}\right) = \left(\frac{N}{N-1}\right)^3\ \ \frac{T_{21\text{ns}} T_{31\text{ws}}\ T_{34\text{ns}}}{T_{21\text{ws}} T_{31\text{ns}}\ T_{34\text{ws}}}. \tag{14}$$

Note that the mean value is biased and a correction factor of $[(N-1)/N]^3$ for the measured mean value is necessary. When substituting $s = 2$ and $s = 3$ into (10), the standard deviation can be derived as

$$\begin{aligned} \text{std}\ \left(x_{\text{SE}}\right) &= \sqrt{M_{XY}\left(3\right) - M_{XY}^2\left(2\right)} \\ &= \left(\frac{N}{N-2}\right)^{\frac{3}{2}} \frac{\left[(N+1)^3(N-1)^3 - (N-2)^3 N^3\right]^{\frac{1}{2}}}{(N-1)^3} \\ &\quad \frac{T_{21\text{ns}} T_{31\text{ws}}\ T_{34\text{ns}}}{T_{21\text{ws}} T_{31\text{ns}}\ T_{34\text{ws}}}. \end{aligned} \tag{15}$$

The relative standard deviation can be obtained from the ratio of (14) and (15), which is

$$\text{std}_{\text{rel}}\ \left(x_{\text{SE}}\right) = \frac{\text{std}}{\text{mean}}\ \times 100\% = \sqrt{\frac{(N-1)^3(N+1)^3}{N^3(N-2)^3} - 1.}. \tag{16}$$

Note that when $N \to \infty$, we have

$$\lim_{N\to\infty} \mu\left(x_{\text{SE}}\right) = \frac{T_{21\text{ns}} T_{31\text{ws}}\ T_{34\text{ns}}}{T_{21\text{ws}} T_{31\text{ns}}\ T_{34\text{ws}}} \tag{17}$$

and

$$\text{std}_{\text{rel}}\left(x_{\text{SE}}\right) \approx \sqrt{\frac{6}{N}}\ . \tag{18}$$

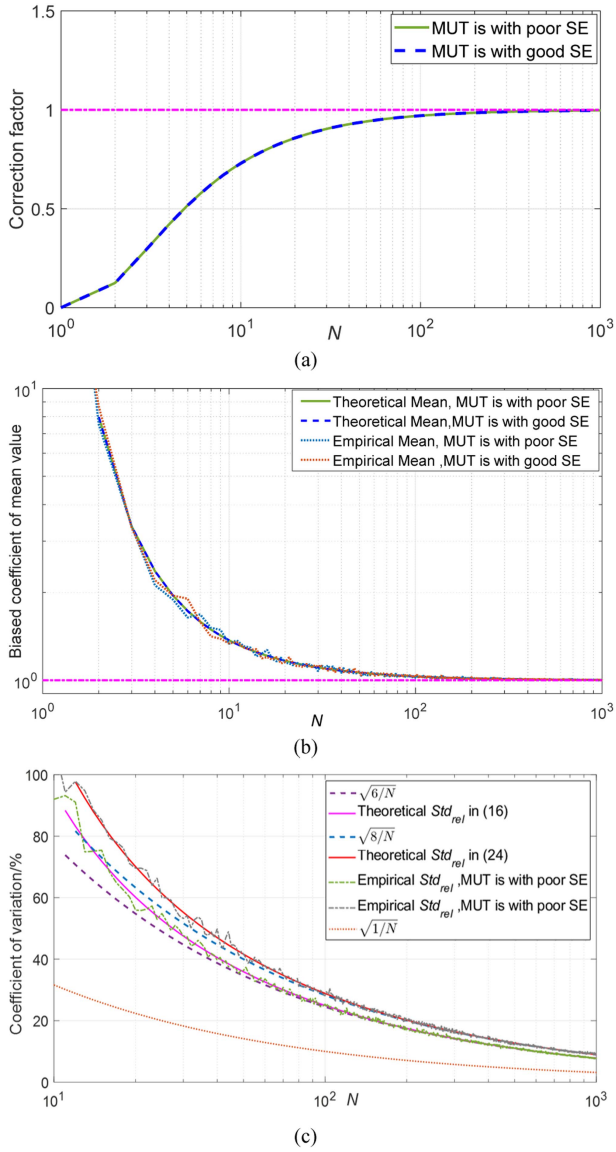

Fig. 3. (a) Correction factor for the MUT with good and poor electromagnetic shielding performance. (b) Biased coefficient of mean value in (14). (c) Curves for $1/\sqrt{N}$, $\sqrt{6/N}$, $\sqrt{8/N}$, the coefficient of variation in (16) and (24), and the empirical standard deviation simulated by Monte Carlo simulations.

The correction factor is given in Fig. 3(a). As expected, when N is larger, the correction factor approaches to 1. The coefficients in (14) and (18) are plotted in Fig. 3(b) and (c), respectively. Note that for finite N samples, the measured SE is not unbiased, but the coefficient in (14) is very close to 1. However, compared with the coefficient of variation from the central limit theorem (CLT) $(1/\sqrt{N})$ [36], for the SE measurement of material in a nested RC, when N is large, a factor of $\sqrt{6}$ is introduced.

B. MUT With Good Electromagnetic Shielding Performance

This section discusses the relevant statistical analysis of the material SE measurement for MUT with good electromagnetic shielding performance in the good stirring nested or contiguous RC. Note that the E-field in the inner and outer chambers is spatially Rayleigh distributed. The variables $|S_{31\text{ns}}|$, $|S_{34\text{ns}}|$, $|S_{21\text{ws}}|$, $|S_{21\text{ns}}|$, and $|S_{34\text{ws}}|$ still are of the same PDF expression, Rayleigh distribution. However, the transmission amplitude coefficient ($|S_{31\text{ws}}|$) between Ant 1 and Ant 3 is double Rayleigh distributed, which can be considered a product of two Rayleigh distributions. So that the PDF of $|S_{31\text{ws}}|^2$ is a product of two exponential distribution, which can be obtained as

$$p_{X_{\text{double}}}(x_{\text{double}}) = \frac{2}{T_{31\text{ws}}^2} K_0\left(\frac{2\sqrt{x_{\text{double}}}}{T_{31\text{ws}}}\right), X_{\text{double}} = |S_{31\text{ws}}|^2 \tag{19}$$

where $K_0(\cdot)$ represents the modified Bessel function of second kind and zeroth order [37]. The integral definition is

$$K_0(\cdot) = \int_0^\infty \cos(x\sinh(t))\,dt = \int_0^\infty \frac{\cos(xt)\,dt}{\sqrt{t^2+1}}. \tag{20}$$

The mean value is $T_{31\text{ws}}^2$, and the standard deviation is $\sqrt{3}T_{31\text{ws}}^2$. The PDF of $\langle|S_{31\text{ws}}|^2\rangle_N$ from N independent samples has no simple analytical expression as the integral cannot be expressed in terms of elementary functions. Nevertheless, the mean and the standard deviation can be derived accordingly as $T_{31\text{ws}}^2$ and $(\sqrt{3}/\sqrt{N})T_{31\text{ws}}^2$ by applying the principles of transformed random variables.

Using (7) and the associated statistical theory [38], the mean value of the variable X_{SE} is obtained as

$$\mu(x_{\text{SE}}) = \left(\frac{N}{N-1}\right)^3 \frac{T_{21\text{ns}}T_{31\text{ws}}^2\,T_{34\text{ns}}}{T_{21\text{ws}}T_{31\text{ns}}\,T_{34\text{ws}}}. \tag{21}$$

And the standard deviation can be derived as

$$\begin{aligned}\text{std}\ (x_{\text{SE}}) &= \text{E}\left(x_{\text{SE}}^2\right) - \text{E}^2\ (x_{\text{SE}}) \\ &= \frac{N^{\frac{3}{2}}\left[(N+1)^2(N-1)^3(N+3) - (N-2)^3N^3\right]^{\frac{1}{2}}}{(N-1)^3(N-2)^{\frac{3}{2}}} \\ &\quad \frac{T_{21\text{ns}}T_{31\text{ws}}^2\,T_{34\text{ns}}}{T_{21\text{ws}}T_{31\text{ns}}\,T_{34\text{ws}}}.\end{aligned} \tag{22}$$

Note that when $N \to \infty$, the approximate mean and standard deviation are

$$\lim_{N\to\infty} \mu(x_{\text{SE}}) = \frac{T_{21\text{ns}}T_{31\text{ws}}^2\,T_{34\text{ns}}}{T_{21\text{ws}}T_{31\text{ns}}\,T_{34\text{ws}}} \tag{23}$$

and

$$\begin{aligned}\lim_{N\to\infty} \text{std}_{\text{rel}}(x_{\text{SE}}) &= \sqrt{\frac{8N^5 - 17N^4 + 4N^3 + 7N^2 + 2N - 3}{N^3(N-2)^3}} \\ &\approx \sqrt{\frac{8}{N}}.\end{aligned} \tag{24}$$

In Fig. 3, the correction factor, the coefficient of the mean, and the standard deviation are presented. The correction factor MUT with good electromagnetic shielding performance is the same as that for MUT with poor electromagnetic shielding performance, and both of them are close to 1. For a small value of N, the SE is biased. For the standard deviation, as shown in Fig. 3(c), the coefficient in (24) is close to the approximate value $\sqrt{8/N}$. The summary of the statistics is shown in Table I. The mean value,

TABLE I
SUMMARY OF THE STATISTICAL EXPRESSION

Statistic	MUT with poor electromagnetic shielding performance	MUT with good electromagnetic shielding performance
Mean value and its approximate expression	$\mu(x_{SE}) = \left(\frac{N}{N-1}\right)^3 \frac{T_{21\text{ns}} T_{31\text{ws}}\, T_{34\text{ns}}}{T_{21\text{ws}} T_{31\text{ns}}\, T_{34\text{ws}}}$ $\lim_{N\to\infty} \mu(x_{SE}) = \frac{T_{21\text{ns}} T_{31\text{ws}}\, T_{34\text{ns}}}{T_{21\text{ws}} T_{31\text{ns}}\, T_{34\text{ws}}}$	$\mu(x_{SE}) = \left(\frac{N}{N-1}\right)^3 \frac{T_{21\text{ns}} T_{31\text{ws}}{}^2\, T_{34\text{ns}}}{T_{21\text{ws}} T_{31\text{ns}}\, T_{34\text{ws}}}$ $\lim_{N\to\infty} \mu(x_{SE}) = \frac{T_{21\text{ns}} T_{31\text{ws}}{}^2\, T_{34\text{ns}}}{T_{21\text{ws}} T_{31\text{ns}}\, T_{34\text{ws}}}$
Standard deviation	$std(x_{SE}) = (\frac{N}{N-2})^{\frac{3}{2}} \frac{[(N+1)^3(N-1)^3 - (N-2)^3N^3]^{\frac{1}{2}}}{(N-1)^3} \frac{T_{21\text{ns}} T_{31\text{ws}}\, T_{34\text{ns}}}{T_{21\text{ws}} T_{31\text{ns}}\, T_{34\text{ws}}}$	$std(x_{SE}) = \frac{N^{\frac{3}{2}}[(N+1)^2(N-1)^3(N+3) - (N-2)^3N^3]^{\frac{1}{2}}}{(N-1)^3(N-2)^{\frac{3}{2}}} \frac{T_{21\text{ns}} T_{31\text{ws}}{}^2\, T_{34\text{ns}}}{T_{21\text{ws}} T_{31\text{ns}}\, T_{34\text{ws}}}$
Approximate expression relative standard deviation	$\lim_{N\to\infty} \text{std}_{\text{rel}}(x_{SE}) \approx \sqrt{\frac{6}{N}}$	$\lim_{N\to\infty} \text{std}_{\text{rel}}(x_{SE}) \approx \sqrt{\frac{8}{N}}$
PDF	$p_{X_{SE}}(x_{SE}) = \frac{\text{MeijerG}[\{\{-N,-N,-N\},\{\}\},\{\{-1+N,-1+N,-1+N\},\{\}\},\frac{x_{SE}}{R}]}{R\Gamma(N)^6}$	

standard deviation, the approximate expression, and the PDF are concluded.

To verify the accuracy of the derived statistic expressions, the Monte Carlo simulations [39], [40], [41], [42], [43] are conducted for different material samples here. For each number of samples N, we randomly generate N independent samples for each variable, $|S_{21\text{ns}}|^2$, $|S_{31\text{ws}}|^2$, $|S_{34\text{ns}}|^2$, $|S_{21\text{ws}}|^2$, $|S_{31\text{ns}}|^2$, and $|S_{34\text{ws}}|^2$, which is the exponential distribution for the MUT with poor electromagnetic shielding performance, or is the exponential distribution or the product of exponential distribution for the MUT with good electromagnetic shielding performance. Here, we suppose that $T_{21\text{ns}}$, $T_{31\text{ws}}$, $T_{34\text{ns}}$, $T_{21\text{ws}}$, $T_{31\text{ns}}$, and $T_{34\text{ws}}$ are 1. Thus, the empirical expectation, relative standard deviation can be obtained.

In Fig. 3(b) and (c), the empirical mean, and relative standard deviation for not well-shielded MUT and well-shielded MUT are presented to verify the correctness of the statistical analysis. These derived statistics are plotted as $N = 1$–10^3.

As demonstrated in Fig. 3(b), the derived mean agrees well with the empirical ones. When N is small, the deviation between the derived one and the simulation one is large. Moreover, the mean value of the two conditions is biased, but the coefficient is the same and close to 1. Note that for a large value of N (no statistical bias), the gap in the statistics between (11) and (19) becomes negligible. The mean value of the SE is $T_{21\text{ns}}T_{31\text{ws}}\ T_{34\text{ns}}/T_{21\text{ws}}T_{31\text{ns}}\ T_{34\text{ws}}$ and $T_{21\text{ns}}T_{31\text{ws}}^2\ T_{34\text{ns}}/T_{21\text{ws}}T_{31\text{ns}}\ T_{34\text{ws}}$, which is equal to 1.

In Fig. 3(c), the empirical standard deviation is in good accordance with the analytical ones. The standard deviation, for the MUT is not well-shielded, is $\sqrt{6/N}$, but for the well-shielded material sample, the coefficient of the value is close to $\sqrt{8/N}$, which means the statistic fluctuation becomes larger. Monte Carlo simulation results verify the correctness of the theoretical derivation.

III. MEASUREMENT RESULTS

In this section, the corresponding measurements of the SE for different MUT in the nested and contiguous RC are performed and the relevant discussions are also given.

A. Measurement in a Nested RC

The whole measurement system in the nested RC is shown in Fig. 1(a). The photographs in Fig. 4 show the configuration of the SE measurements in a nested RC. The dimension of the outer chamber is 3.9 m $\times$ 6 m $\times$ 2.8 m, and that of the inner chamber is 0.6 m $\times$ 0.45 m $\times$ 0.46 m.

During the whole testing procedure, four antennas are used: Ant 1 and Ant 2 are wideband dipole antennas, which are supported in the outer cavity utilizing two fixtures with adjustable orientation and height. Ant 3 and Ant 4 are dipole antennas different from the former and are placed in the inner cavity, as shown in Fig. 4(b). Ant 1 (or Ant 4) is connected to the VNA Port 1 and Ant 2 is connected (or Ant 3) to the VNA Port 2. The antennas not connected to the VNA should be connected on a 50-Ω load. The antennas are located at a sufficient distance (at least $\lambda/4$) from the RC walls and the stirrers. Note that for the nested RC, the outer chamber has two stirrers, vertical and horizontal, and the inner chamber has one vertical stirrer. The step rotation of the stirrer is synchronized. In the measurements, 360 samples for each measurement are shown in Fig. 4(b) (1 °/step for all horizontal and vertical stirrers). For each step of three stirrers, the computer records the measured *S*-parameters from the VNA.

To obtain the material samples with good and poor electromagnetic shielding performance, the measurements are performed using different samples. When no sample in the testing system, corresponding to the subscript "ns," the $S_{31\text{ns}}$, $S_{34\text{ns}}$, and $S_{21\text{ns}}$ are the same for different samples. After placing the

(a)

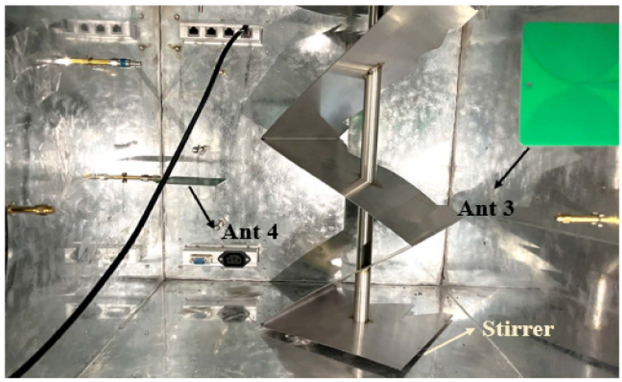

(b)

Fig. 4. Measurement setup in the nested RC experiment. (a) Typical measurement system; the dimension of the outer chamber is 3.9 m × 6 m × 2.8 m. (b) Antenna 3 and antenna 4 in the inner chamber, and its dimension is 0.6 m × 0.45 m × 0.46 m. The size of the aperture is 0.36 m × 0.26 m.

material samples in a nested RC, repeat the above steps and obtain $S_{31\mathrm{ws}}$, $S_{34\mathrm{ws}}$, and $S_{21\mathrm{ws}}$. A total of 6001 frequency points are recorded for each stirrer position in the frequency range between 1 and 6 GHz.

The *S*-parameters without the MUT with poor electromagnetic shielding performance and with good electromagnetic shielding performance are given in Fig. 5(a)–(c). Measurement results and the corrected SE in dB form are shown in Fig. 5(d), which are used to generate the measured CDFs of the SE in the nested RC from 1 to 6 GHz. Moreover, N was estimated through the fluctuation of SE. The corrected factor and the corrected SE can be calculated. The corrected SE is in accordance with the measured SE, although some fluctuation occurred.

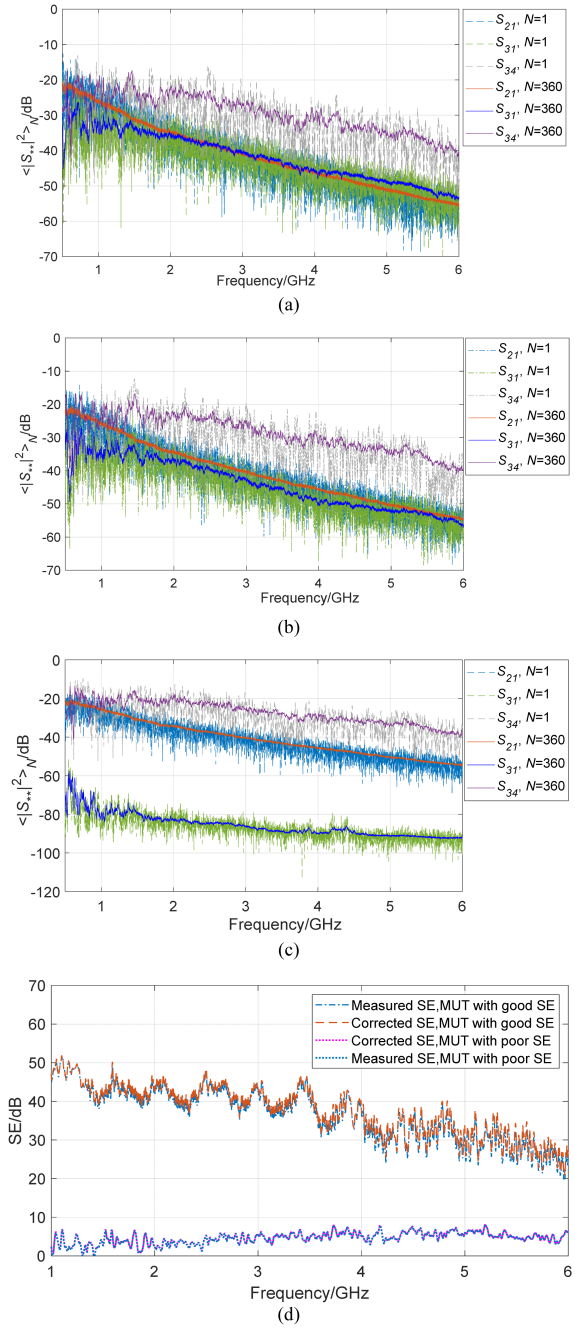

Fig. 5. Measured results of the sample in the nested RC from 1 to 6 GHz. (a) *S*-parameters without the MUT. (b) *S*-parameters for the MUT with poor electromagnetic shielding performance. (c) *S*-parameters for the MUT with good electromagnetic shielding performance. (d) Measured SE and the corrected SE in dB form.

B. Measurement in a Contiguous RC

This section presents the performed measurement of the SE in the contiguous RC. The testing setup is given in Fig. 1(b). In Fig. 6(a) and (b), the measurement setup details of the two chambers are shown, whose dimensions are 5.1 m × 3.9 m × 2.95 m and 4.65 m × 3.9 m × 2.95 m, respectively. Moreover, the aperture is 1 m × 1 m. The photographs of the aperture with MUT and without MUT are also given in Fig. 6(c) and (d).

The testing procedure in the contiguous RC is similar to that in the nested RC. Four antennas are used as Tx antennas and Rx antennas here, marked as Ant 1, Ant 2, Ant 3, and Ant 4. Note that for the contiguous RC system, each chamber has two stirrers, vertical and horizontal. During the testing procedure, four stirrers are used. A total of 6001 frequency points from 0.2 to 6 GHz were recorded.

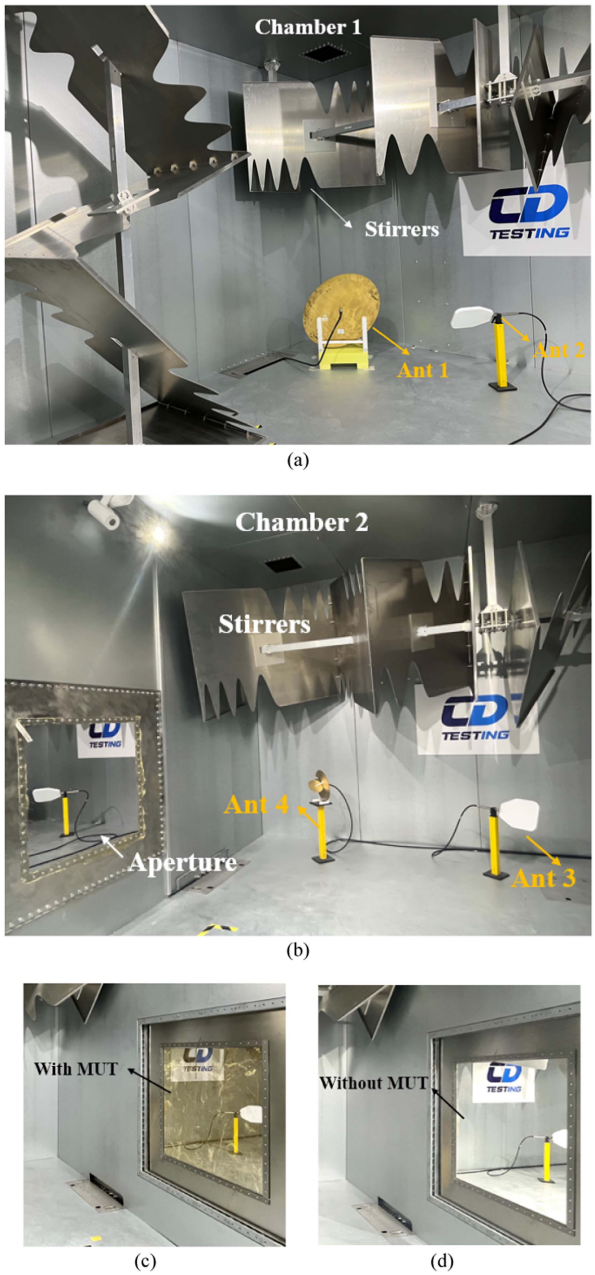

Fig. 6. Measurement setup in the contiguous RC experiment. (a) Typical measurement system in the left chamber, and its dimension is 5.1 m × 3.9 m × 2.95 m (b) in the right chamber, and its dimension is 4.65 m × 3.9 m × 2.95 m. Details of the configuration (c) with MUT and (d) without MUT. The size of the aperture is 1 m × 1 m.

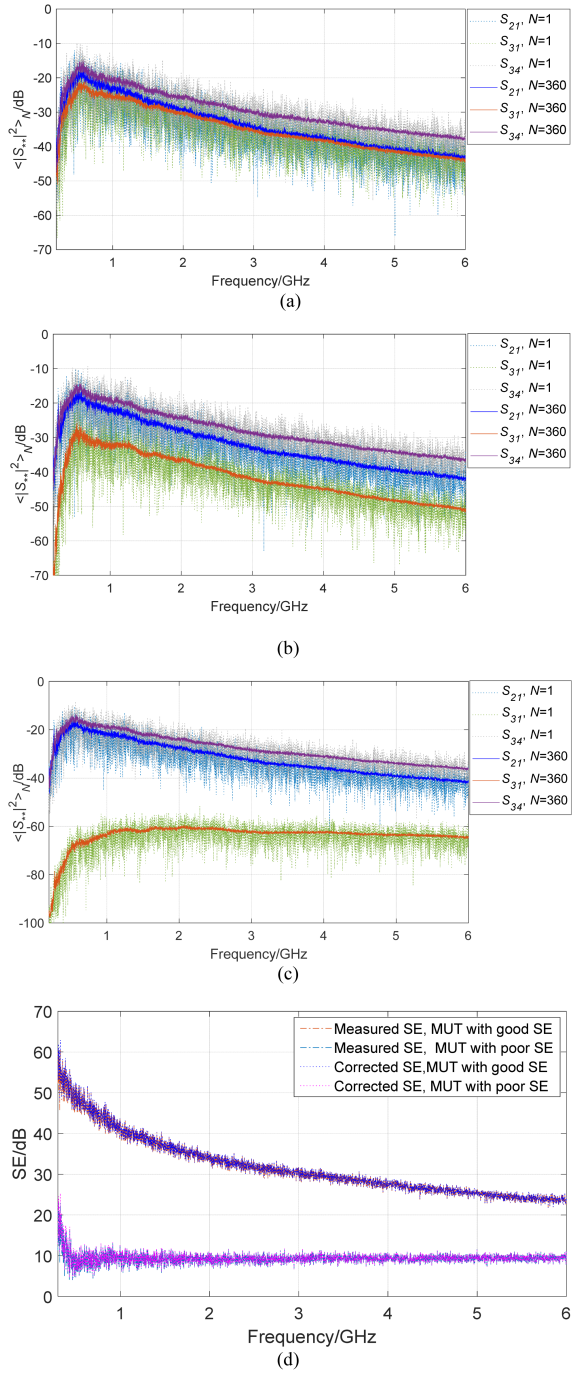

Fig. 7. Measured results of the sample in the contiguous RC from 0.2 to 6 GHz. (a) *S*-parameters without the MUT. (b) *S*-parameters for the MUT with poor electromagnetic shielding performance. (c) *S*-parameters for the MUT with good electromagnetic shielding performance. (d) Measured SE and the corrected SE in dB form.

The measured *S*-parameters $\langle|S_{21\text{ws}}|^2\rangle_N$, $\langle|S_{31\text{ws}}|^2\rangle_N$, $\langle|S_{34\text{ws}}|^2\rangle_N$, $\langle|S_{21\text{ns}}|^2\rangle_N$, $\langle|S_{31\text{ns}}|^2\rangle_N$, and $\langle|S_{34\text{ns}}|^2\rangle_N$ are shown when $N = 1$ and $N = 360$ in Fig. 7(a)–(c). Testing and the corrected SE in dB form for MUT with different SE are given in Fig. 7(d) in the contiguous RC. N is also estimated through by the fluctuation of SE in the frequency range between 1 and 6 GHz. Thus, the corrected SE can also be obtained. It is observed that small deviations exist between the measured SE and the corrected SE.

The analytical and the measured CDFs in the nested RC and the contiguous RC are then given in Figs. 8 and 9. As expected, in Figs. 8(a) and 9(a), the analytical and the measurement results agree well for the MUT with poor electromagnetic shielding performance. A small deviation exists because of the finite samples. When N increases, the deviation becomes smaller.

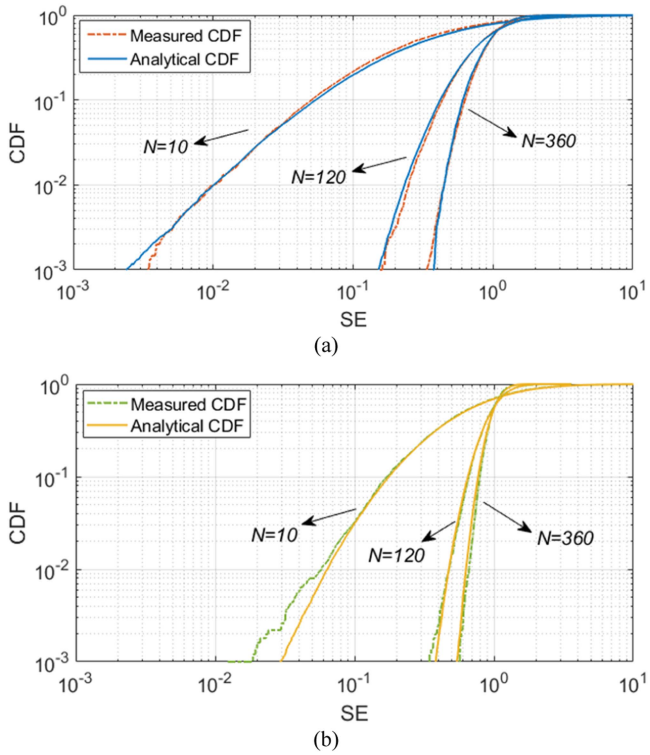

Fig. 8. Comparison of analytical and measured CDF of the not well-shielded sample with $N = 10, 120$, and 360 (a) in the nested RC and (b) in the contiguous RC.

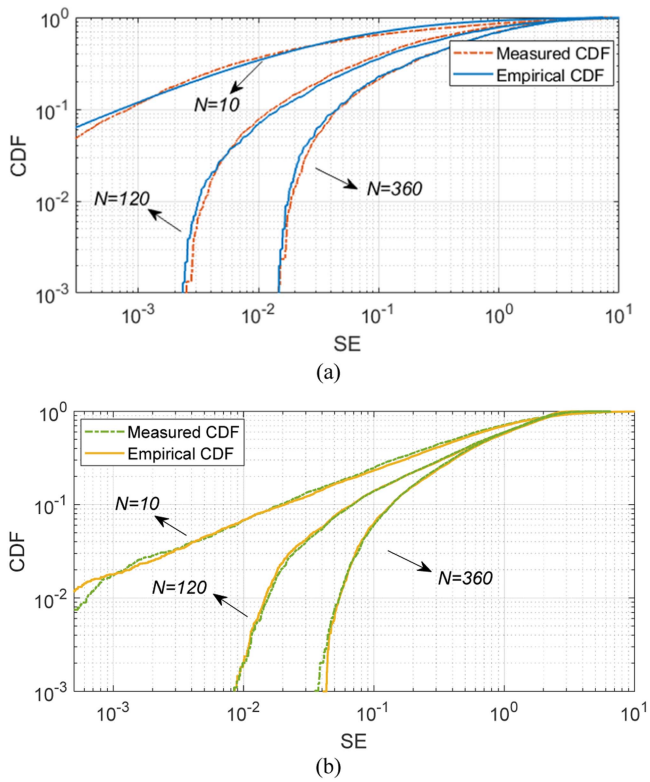

Fig. 9. Comparison of empirical and measured CDF of the MUT with good electromagnetic shielding performance with $N = 10$, 120, and 360 (a) in the nested RC and (b) in the contiguous RC.

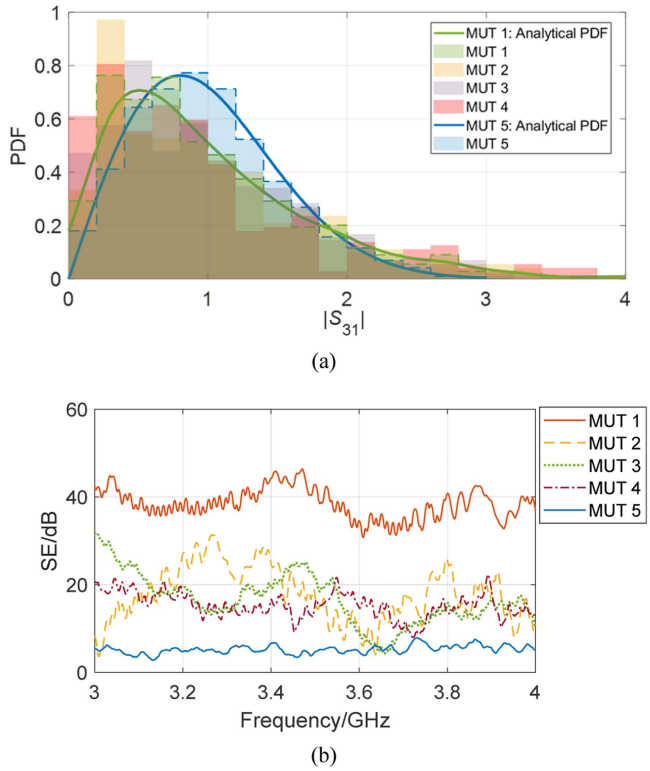

Fig. 10 (a) Measured PDF of $|S_{31ws}|$. (b) Measured SE for different MUT from 3 to 4 GHz.

Moreover, the empirical results and the measurement results for the MUT with good electromagnetic shielding performance are also presented due to the lack of simple expressions. It is shown that under different N, the curves agree well.

In Figs. 8(b) and 9(b), we compare the analytical results, the empirical results, and the measurement results in a different stirring position in the contiguous RC. The analytical and measurement results are consistent with each other. When $N = 10$, the deviation of the curves occurs. As N increase, the deviation becomes smaller. Moreover, the empirical and the measurement CDFs of the MUT with good electromagnetic shielding performance agree well.

Compared to the measurement results in the nested and the contiguous RC, the measured CDFs agree well with the theoretical CDFs for the MUT with poor electromagnetic shielding performance or the empirical CDFs for the MUT with good electromagnetic shielding performance. When N is small, some deviations occur and the statistics are biased. The measurement results also verify the correctness of the theoretical derivation.

Also, it is observed that for the transition $|S_{31\mathrm{ws}}|$ between these Rayleigh distribution and double Rayleigh distribution, both hypotheses are found inappropriate. As shown in Fig. 10(a), the PDFs of $|S_{31\mathrm{ws}}|$ at 3.5 GHz are given. Note that MUT 1 is with good shielding electromagnetic performance, MUT 5 is with poor shielding electromagnetic performance. By tuning the number of holes of the MUT, three transition states are defined as MUT 2, MUT 3, and MUT 4.

TABLE II
REJECTION RATE OF BOTH HYPOTHESES WITH DIFFERENT MUT

Statistic		MUT1	MUT2	MUT3	MUT4	MUT5
Rayleigh distribution	K-S test	96.3%	96.0%	94.6%	70.4%	2.1%
	χ^2 test	96.7%	95.8%	95.1%	69.9%	1.8%
Double Rayleigh distribution	K-S test	3.3%	60.8%	87.0%	92.6%	97.2%
	χ^2 test	2.9%	61.7%	86.4%	93.5%	98.1%

We performed the Kolmogorov–Smirnov (K-S) test and Chi-squared (χ^2) test for different MUTs. For MUT 1 and MUT 5, the rejection rates in Table II show that both K-S test and Chi-squared test fails to reject the hypothesis at a 5% significance level. That is, when MUT is with poor electromagnetic shielding performance, $|S_{31\text{ws}}|$ is Rayleigh distribution; when MUT is with good electromagnetic shielding performance, $|S_{31\text{ws}}|$ is double Rayleigh distribution.

For the transition state of Rayleigh distribution and double Rayleigh distribution, according to CLT, suppose that $\langle|S_{31\text{ws}}|^2\rangle_N$ is normal distribution, the mean of $\langle|S_{31\text{ws}}|^2\rangle_N$ is $\mu_{31\text{ws}}$, and the standard deviation is $\sigma_{31\text{ws}}/\sqrt{N}$. Note that if the CLT is used, no simple PDF expressions of SE can be obtained as the integral cannot be evaluated in a closed form. Fig. 10(b) shows the measured SE from 3 to 4 GHz.

Then, we try to derive relative standard deviation of SE for different MUT, which is the ratio of standard deviation and mean. Suppose that the linear form of $\text{SE} = x_1\, x_2 x_3/x_4 x_5 x_6$, where $x_1 = T_{21\text{ns}},\ x_2 = T_{31\text{ws}},\ x_3 = T_{34\text{ns}},\ x_4 = T_{21\text{ws}},\ x_5 = T_{31\text{ns}}$, and $x_6 = T_{34\text{ws}}$. The standard deviation of x_2 is $\sigma_{31\text{ws}}/\sqrt{N}$ and the standard deviation of other term is $\text{std}\,(x_i) = x_i\,/\sqrt{N}, i = 1,\ 3,\ 4,\ 5,\ 6$.

Using the propagation of uncertainty equation [44], [45], [46], the standard deviation can be derived as

$$\text{std}\,(x_{\text{SE}}) \approx \sqrt{\sum\nolimits_{i=1}^{6}\left[\frac{\partial \text{SE}}{\partial x_i}\text{std}(x_i)^2\right]}. \tag{25}$$

Then, substitute the standard deviation of each term; thus, the relative standard deviation can be obtained as

$$\text{std}_{\text{rel}}\ (x_{\text{SE}}) = \frac{\text{std}\,(x_{\text{SE}})}{\text{SE}} \approx \sqrt{\frac{5}{N} + \frac{\sigma_{31\text{ws}}^2}{T_{31\text{ws}}^2 N}}. \tag{26}$$

Note that the relative standard deviation depends on the ratio of $T_{31\text{ws}}$ and $\sigma_{31\text{ws}}$. When MUT is with poor electromagnetic shielding performance, for $\langle|S_{31\text{ws}}|^2\rangle_N$, the mean value is $T_{31\text{ws}}$ and the standard deviation is $T_{31\text{ws}}/\sqrt{N}$; thus, $\text{std}_{\text{rel}}(x_{\text{SE}})$ is approximately equal to $\sqrt{6/N}$, which is equal to the approximate value in (18). Moreover, when MUT is with good electromagnetic shielding performance, $\text{std}_{\text{rel}}(x_{\text{SE}})$ is approximately equal to $\sqrt{8/N}$, which is equal to the approximate value in (24).

IV. CONCLUSION

In this article, we have analyzed and derived the statistical distributions of the SE for the MUT with good and poor electromagnetic shielding performance, respectively. Using the Mellin transform and corresponding transformed variables methods, the statistics of the SE, such as mean and standard deviation, and their approximate expressions are given. It is interesting to note that the PDF of the measured SE depends on the shielding ability of the MUT. The analytically derived statistics are verified by simulation and experiments. Results in the nested and contiguous RC both show good agreements with the theory.

The analysis results show that when N is small, the mean value is biased for the MUT. It is interesting to find that the correction factors of these two conditions are the same, which are both $[(N-1)/N]^3$. When N becomes larger, the mean value of the measurement SE is very close to the expected value (almost unbiased) whereby the standard deviations are $\sqrt{6/N}$ and $\sqrt{8/N}$, respectively. The analytical expressions derived in this article give rigorous uncertainty analysis of the SE of materials. Using the propagation of the uncertainty equation, for the transition state, the relative standard deviation is also derived.

REFERENCES

[1] R. W. Evans, "Design guidelines for shielding effectiveness, current carrying capability, and the enhancement of conductivity of composite materials," NASA, Washington, DC, USA, NASA Contractor Rep. 4784, Aug. 1997.
[2] K. F. Casey, "Advanced composite materials and electromagnetic shielding," in *Proc IEEE Int. Symp. Electromagn. Compat.*, 1978, pp. 228–232.
[3] C. L. Holloway, D. A. Hill, J. Ladbury, G. Koepke, and R. Garzia, "Shielding effectiveness measurements of materials using nested reverberation chambers," *IEEE Trans. Electromagn. Compat.*, vol. 45, no. 2, pp. 350–356, May 2003.
[4] *ASTM-ES7 and ASTM-D4935 Standard for Measuring the Shielding Effectiveness in the Far Field, vol. 10.02*, ASTM, Philadelphia, PA, USA, 1995.
[5] P. F. Wilson and M. T. Ma, "Techniques for measuring the electromagnetic shielding effectiveness of materials—Part II: Near-field source simulation," *IEEE Trans. Electromagn. Compat.*, vol. 30, no. 3, pp. 251–259, Aug. 1988.
[6] A. Gifuni et al., "On the shielding effectiveness calculation of enclosures through measurements in reverberation chambers," *IEEE Trans. Electromagn. Compat.*, vol. 63, no. 5, pp. 1395–1406, Oct. 2021.
[7] A. Gifuni et al., "Nondestructive reverberation chamber measurement of microwave oven total radiated power and shielding effectiveness," *IEEE Trans. Electromagn. Compat.*, vol. 63, no. 2, pp. 427–434, Apr. 2021.
[8] C. L. Holloway et al., "Use of reverberation chambers to determine the shielding effectiveness of physically small, electrically large enclosures and cavities," *IEEE Trans. Electromagn. Compat.*, vol. 50, no. 4, pp. 770–782, Nov. 2008.
[9] J. H. Hwang, H. H. Park, C. H. Hyoung, and J. H. Kwon, "Quality factor and shielding effectiveness measurement of an antenna-free enclosure in a nested reverberation chamber," *IEEE Trans. Electromagn. Compat.*, vol. 62, no. 6, pp. 2358–2367, Dec. 2020.
[10] A. Gifuni, "A proposal to improve the standard on the shielding effectiveness measurements of materials and gaskets in a reverberation chamber," *IEEE Trans. Electromagn. Compat.*, vol. 59, no. 2, pp. 394–403, Apr. 2017.
[11] R. Araneo and G. Lovat, "Fast MoM analysis of the shielding effectiveness of rectangular enclosures with apertures, metal plates, and conducting objects," *IEEE Trans. Electromagn. Compat.*, vol. 51, no. 2, pp. 274–283, May 2009.
[12] J. H. Hwang, H. H. Park, C. H. Hyoung, and J. H. Kwon, "Shielding effectiveness measurement with wide dynamic range for a small enclosure in a nested reverberation chamber," *IEEE Trans. Electromagn. Compat.*, vol. 63, no. 5, pp. 1407–1416, Oct. 2021.
[13] M. Pocai, I. Dotto, and D. Festa, "Three methods for measuring the shielding effectiveness of shielding materials: A comparison," in *Proc. IEEE Int. Symp. Electromagn. Compat.*, 2012, pp. 663–668.
[14] *Electromagnetic Compatibility (EMC) – Part 4-21: Testing and Measurement Techniques–Reverberation Chamber Test Methods*, IEC Standard, IEC 61000-4-21, Ed 2.0, 2011-01.

[15] *IEEE Standard Method for Measuring the Effectiveness of Electromagnetic Shielding Enclosures*, IEEE Standard 299-1997, 1997.
[16] D. A. Hill, *Electromagnetic Fields in Cavities: Deterministic and Statistical Theories*. Hoboken, NJ, USA: Wiley, 2009.
[17] Q. Xu and Y. Huang, *Anechoic and Reverberation Chambers: Theory, Design and Measurements*. U.K.: Wiley-IEEE, 2019.
[18] W. Qi, F. Fang, W. Xia, Y. Zhao, L. Xing, and Q. Xu, "A compact multi-probe reverberation chamber for over-the-air testing," *ACES J.*, vol. 36, no. 9, pp. 1196–1201, 2021.
[19] X. Chen et al., "Reverberation chambers for over-the-air tests: An overview of two decades of research," *IEEE Access*, vol. 6, pp. 49129–49143, 2018.
[20] Q. Xu, Y. Huang, X. Zhu, L. Xing, Z. Tian, and C. Song, "A modified two-antenna method to measure the radiation efficiency of antennas in a reverberation chamber," *IEEE Antennas Wireless Propag. Lett.*, vol. 15, pp. 336–339, 2016.
[21] T. A. Loughry and S. H. Gurbazani, "The effects of intrinsic test fixture isolation on material shielding effectiveness measurements using nested mode-stirred chambers," *IEEE Trans. Electromagn. Compat.*, vol. 37, no. 3, pp. 449–452, Aug. 1995.
[22] B. Foulonneau, F. Gaudaire, and Y. Gabillet, "Measurement method of electromagnetic transmission loss of building components using two reverberation chambers," *Electron. Lett.*, vol. 32, no. 23, pp. 2130–2131, 1996.
[23] A. Gifuni and M. Migliaccio, "Use of nested reverberating chambers to measure shielding effectiveness of nonreciprocal samples taking into account multiple interactions," *IEEE Trans. Electromagn. Compat.*, vol. 50, no. 4, pp. 783–786, Nov. 2008.
[24] M. O. Hatfield, "Shielding effectiveness measurements using mode-stirred chambers: A comparison of two approaches," *IEEE Trans. Electromagn. Compat.*, vol. 30, no. 3, pp. 229–238, Aug. 1988.
[25] W. Kurner and A. Schwab, "Parameters and results of SE-measurements performed in mode-stirred chambers," in *Proc. IEEE Int. Symp. Electromagn. Compat. Symp. Rec.*, 2000, pp. 611–614.
[26] M. Höijer and L. Kroon, "Field statistics in nested reverberation chambers," *IEEE Trans. Electromagn. Compat.*, vol. 55, no. 6, pp. 1328–1330, Dec. 2013.
[27] A. Gifuni, "Probability density function of the quality factor for reverberation chambers operating with hybrid stirring including frequency stirring," *IEEE Trans. Electromagn. Compat.*, vol. 58, no. 3, pp. 919–922, Jun. 2016.
[28] L. R. Arnaut, M. I. Andries, J. Sol, and P. Besnier, "Evaluation method for the probability distribution of the quality factor of mode-stirred reverberation chambers," *IEEE Trans. Antenna Propag.*, vol. 62, no. 8, pp. 4199–4208, Aug. 2014.
[29] Q. Xu, L. Xing, Y. Zhao, T. Jia, and Y. Huang, "Probability distributions of three-antenna efficiency measurement in a reverberation chamber," *IET Microw. Antennas Propag.*, vol. 15, pp. 1545–1552, 2021.
[30] X. Chen, "Measurement uncertainty of antenna efficiency in a reverberation chamber," *IEEE Trans. Electromagn. Compat.*, vol. 55, no. 6, pp. 1331–1334, Dec. 2013.
[31] W. Xue, X. Chen, M. Zhang, L. Zhao, A. Zhang, and Y. Huang, "Statistical analysis of antenna efficiency measurements with non-reference antenna methods in a reverberation chamber," *IEEE Access*, vol. 8, pp. 113967–113980, 2020.
[32] Q. Xu et al., "Statistical distribution of the enhanced backscatter coefficient in reverberation chamber," *IEEE Trans. Antennas Propag.*, vol. 66, no. 4, pp. 2161–2164, Apr. 2018.
[33] A. Gifuni et al., "On the improvement of shielding effectiveness measurements of materials and gaskets in reverberation chambers," *IEEE Trans. Electromagn. Compat.*, vol. 64, no. 5, pp. 1653–1664, Oct. 2022, doi: 10.1109/TEMC.2022.3193191.
[34] Y. A. Brychkov, O. I. Marichev, and N. V. Savischenko, *Handbook of Mellin Transforms*. London, U. K.: Chapman and Hall/CRC, 2018.
[35] F. Oberhettinger, *Tables of Mellin Transforms*. Berlin, Germany: Springer, 1974.
[36] F. W. Olver, D. W. Lozier, R. F. Boisvert, and C. W. Clark, *NIST Handbook of Mathematical Functions*. Cambridge, U.K.: Cambridge Univ. Press. 2010.
[37] F. Bowman, *Introduction to Bessel Functions*. North Chelmsford, U.K.: Courier Corporation, 2012.
[38] A. Gifuni, A. Sorrentino, G. Ferrara, and M. Migliaccio, "An estimate of the probability density function of the sum of a random number of independent random variables," *J. Comput. Eng.*, vol. 2015, 2015, Art. no. 12.
[39] Y. He and A. C. Marvin, "Aspects of field statistics inside nested frequency-stirred reverberation chambers," in *Proc. IEEE Int. Symp. Electromagn. Compat.*, 2009, pp. 171–176.
[40] G. Gradoni, T. M. Antonsen, S. M. Anlage, and E. Ott, "A statistical model for the excitation of cavities through apertures," *IEEE Trans. Electromagn. Compat.*, vol. 57, no. 5, pp. 1049–1061, Oct. 2015.
[41] M. Magdowski, S. V. Tkachenko, and R. Vick, "Coupling of stochastic electromagnetic fields to a transmission line in a reverberation chamber," *IEEE Trans. Electromagn. Compat.*, vol. 53, no. 2, pp. 308–317, May 2011.
[42] J. M. Ladbury, "Monte Carlo simulation of reverberation chambers," in *Proc. 18th Digit. Avionics Syst. Conf., Gateway New Millennium*, 1999, pp. 10.C.1–10.C.1.
[43] L. Musso, V. Berat, F. Canavero, and B. Demoulin, "A plane wave Monte Carlo simulation method for reverberation chambers," in *Proc. Int. Symp. Electromag. Compat.*, 2002, vol. 1, pp. 45–50.
[44] S. Bell, *The Beginner's Guide to Uncertainty of Measurement*. Teddington, U.K.: Nat. Phys. Lab., 2011.
[45] K. Birch, *Estimating Uncertainties in Testing*. Guildford, U.K.: British Measurement and Testing Association, 2003.
[46] R. Willink, *Measurement Uncertainty and Probability*. Cambridge, U.K.: Cambridge Univ. Press, 2013.

Wenjun Qi received the B.Eng. and M.Eng. degrees in microwave technology from the Nanjing University of Aeronautics and Astronautics, Nanjing, China, in 2018 and 2021, respectively. She is currently working toward the Ph.D. degree in electromagnetic field and microwave technology from Nanjing University of Aeronautics and Astronautics.

Her main research interests include reverberation chamber, computational electromagnetics and statistical electromagnetics, over-the-air (OTA) testing, and electromagnetic compatibility (EMC).

Kai Chen received the M.Eng. degree in agricultural mechanization from Yangtze University, Jingzhou, China, in 2014. He is currently working toward the Ph.D. degree in electromagnetic field and microwave technology with the College of Electronic and Information Engineering, Nanjing University of Aeronautics and Astronautics, Nanjing, China.

He was an EMC Engineer with H3C, Hangzhou, China, in 2010. He is currently an Application Engineer with Nanjing Rongce Testing Technology Ltd., Nanjing. His main research interests include reverberation chamber and electromagnetic compatibility (EMC).

Xueqi Shen received the M.Eng. degree in electrical engineering and electronics from the Department of Radio, Southeast University, Nanjing, China, in 1989.

In 2004, he founded Rongxiang Company and in 2012, Nanjing Rongce Testing Technology Ltd., which is a recognized EMC laboratory by Ford and Yutong. Currently, Nanjing Rongce has the largest vehicle reverberation chamber in China.

Mr. Shen is currently a Committee Member of Branches A, I, and D of the National Technical Committee on Radio Interference of Standardization Administration of China.

Yongjiu Zhao received the M.Eng. and Ph.D. degrees in electronic engineering from Xidian University, Xi'an, China, in 1990 and 1998, respectively.

Since March 1990, he has been with the Department of Mechano-Electronic Engineering, Xidian University, where he was a professor in 2004. From December 1999 to August 2000, he was a Research Associate with the Department of Electronic Engineering, The Chinese University of Hong Kong. His research interests include antenna design, microwave filter design, and electromagnetic theory.

Qian Xu (Member, IEEE) received the B.Eng. and M.Eng. degrees in electrical engineering and electronics from the Department of Electronics and Information, Northwestern Polytechnical University, Xi'an, China, in 2007 and 2010, and the Ph.D. degree in electrical engineering from the University of Liverpool, U.K., in 2016.

He was as an RF engineer in Nanjing, China, in 2011, an Application Engineer with CST Company, Shanghai, China, in 2012. He is currently an Associate Professor with the College of Electronic and Information Engineering, Nanjing University of Aeronautics and Astronautics, Nanjing, China. His work at University of Liverpool was sponsored by Rainford EMC Systems Ltd. (now part of Microwave Vision Group) and Centre for Global Eco-Innovation. He has designed many chambers for the industry and has authored the book *Anechoic and Reverberation Chambers: Theory, Design, and Measurements* (Wiley-IEEE, 2019). His research interests include statistical electromagnetics, reverberation chamber, EMC, and over-the-air testing.

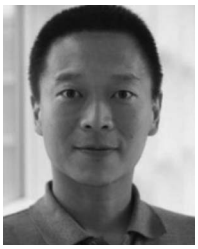

Tian Hong Loh (Senior Member, IEEE) received the Ph.D. degree in engineering from the University of Warwick, Coventry, U.K., in 2005.

Since 2005, he has been with the National Physical Laboratory (NPL), Teddington, U.K., where he is currently the Principal Research Scientist. He leads work at NPL on a wide range of applied electromagnetic metrology research areas to support the telecommunications industry. He is also a Visiting Professor with Surrey University, Guildford, U.K., a Visiting Industrial Fellow with Cambridge University, Cambridge, U.K., and Secretary of URSI U.K. Panel. He holds six patents, one edited book *Metrology for 5G and Emerging Wireless Technologies* (IET, 2021), nine book chapters, and has authored and coauthored more than 180 refereed publications. His research interests include 5G/6G communications, smart antennas, small antennas, metamaterials, body-centric communications, wireless sensor networks, electromagnetic compatibility, and computational electromagnetics.

Yi Huang (Fellow, IEEE) received the B.Sc. degree in physics from Wuhan University, Wuhan, China, in 1984, the M.Sc. (Eng.) degree in microwave engineering from the Nanjing Research Institute of Electronics Technology (NRIET), Nanjing, China, in 1987, and the D.Phil. degree in communications from the University of Oxford, Oxford, U.K., in 1994.

His experience includes three years spent with NRIET, China, as a Radar Engineer, and various periods with the Universities of Birmingham, Oxford, and Essex, in the U.K., as a Research Staff Member. In 1994, he was a Research Fellow with British Telecom Labs, and then, in 1995, he joined as a Faculty the Department of Electrical Engineering and Electronics, University of Liverpool, U.K., where he is currently a Full Professor in wireless engineering, the Head of the High Frequency Engineering Group, and the Deputy Head of the Department. He has authored or coauthored more than 400 refereed articles in leading international journals and conference proceedings, and authored three books, including a bestseller *Antennas: From Theory to Practice* (John Wiley, 2008, 2021). He has received many patents, and research grants from research councils, government agencies, charity, EU, and industry. His research interests include antennas, wireless communications, applied electromagnetics, radar, and EMC, with current focus on mobile antennas, wireless energy harvesting, and power transfer.

Dr. Huang is the U.K. and Ireland Representative of the European Association of Antenna and Propagation (EurAAP) for the period 2016–2020 and a Fellow of IET. He was the recipient of more than ten awards, such as the BAE Systems Chairman's Award 2017, the IET, and the Best Paper Awards. He was on a number of national and international technical committees and been an Editor, an Associate Editor, or a Guest Editor for five international journals. He is the Editor-in-Chief of *Wireless Engineering and Technology* and an Associate Editor for IEEE ANTENNAS AND WIRELESS PROPAGATION LETTERS. In addition, he has been a Keynote/an Invited Speaker and an Organizer of many conferences and workshops, such as IEEE iWAT2010, LAPC2012, and EuCAP2018.